Modeling the Contribution of Diffusion to Device Upset Cross Sections

J. D. Patterson
L. D. Edmonds
Jet Propulsion Laboratory, California Institute of Technology, Pasadena, Ca, 91109

A novel technique, incorporating mixed boundary conditions and carrier recombination, for determining the diffusion charge collection efficiency function, $\Omega_\tau(\vec{x})$, is presented and applied to a realistic, 3-D, memory device, to obtain the upset cross section, σ, as a function of LET and orientation of incidence. The model is able to reproduce experimental measurements, and can be used to more accurately predict σ across regimes where little data exists. This will allow for the determination of more precise errors rates, while simultaneously requiring fewer experimental data points.

I. Introduction

Historically, many of the attempts to predict heavy ion-induced upset cross sections, σ, have been based solely on geometrical considerations, with minimal input from semiconductor physics. The Rectangular Parallelepiped (RPP) [1] and its more sophisticated counterpart, the Heavy Ion Cross Section for Single Event Upset (HICUP), [2] and [3], have been popular constructs used to model σ and calculate device upset rates for many years. Although these approaches have been successful in replicating experimental measurements when model parameters are selected to fit data, the limited physical input leaves their applicability to future volatile memory devices somewhat limited.

In recent years, efforts to construct charge collection models governed by the charge transport equations incorporating carrier recombination and drift/diffusion have been undertaken by various members of the SEE community. Due to the wide availability of sophisticated packages that employ finite element analysis to solve the Poisson and continuity equations, much has been learned regarding the evolution of injected charge in a device via computer simulations, [4] and [5]. However, full 3-D simulation codes are computationally intensive, so a great deal of effort and machine time are needed to predict upset cross section as a function of ion LET and incident angle, even for simple, single or double junction devices. The computational intensity for more complex devices, such as DRAMs, that contain millions of cells and have the property that charge can travel great distances from an ion track to upset a particular cell, can be overwhelming.

The research described in this paper was carried out by the Jet Propulsion Laboratory, California Institute of Technology, under a contract with the National Aeronautics and Space Administration. Reference herein to any specific commercial product, process, or service by trade name, trademark, manufacturer, or otherwise, does not constitute or imply its endorsement by the United States Government or the Jet Propulsion Laboratory, California Institute of Technology.

Other authors such as Kirkpatrick [11], Wouters [12], Smith et al. [7], and Edmonds [8] and [9] have used a more analytic approach intended for those cases in which diffusion is believed to be the dominant charge transport mechanism. The first three authors assumed Dirichlet-only type boundary conditions on the entire upper device plane (the cell density is large enough for adjacent cells to share boundaries). Edmonds used the more versatile mixed-type boundary conditions, but his treatment still contained unrealistic simplifications (an entire array of cells is replaced by several types of regions defined by concentric rings). Also, while Edmonds treated recombination in the theory [8], this was not included in the numerical results. A more recent paper [10] removes these limitations only if the reader can supply information that is difficult to obtain and is unique to the geometry of interest.

Like the earlier treatments, it is assumed here that charge transport is governed by diffusion. The charge-collection time is assumed in this work to be effectively infinite, so the applicability of this work is somewhat limited. A notable example in which this work is believed to be relevant is the DRAM. It has been known for some time that diffusion can transport charge over large distances in DRAMs [6]. A notable distinction between this work and previous work is in the assumed boundary conditions.

The present paper is the first to use mixed boundary conditions that give a literal representation of a large array of cells of arbitrary aspect ratio and spacings. The mixed boundary conditions include reflective boundary conditions between cells. This is essential for predicting that different cells each collect a portion of charge liberated between cells near the top of the device. In contrast, the Dirichlet-type conditions used in previous work predict that all charge liberated near the top of the device is collected entirely by one cell. Furthermore, recombination is included in the numerical results.

Ultimately, cross sections are measured to provide the device inputs for upset rate calculations. In order to carry out the folding integrals, the cross section must be evaluated at all environmentally relevant ion LETs and orientations. However, due to practical considerations, measurements can be obtained at only a handful of LETs and angles. In practice, LET and orientation are combined into a single variable:"effective LET", via the cosine law. However, the cosine law is a very poor approximation for at least some DRAMs [13]. When the cosine law fails, ion

LET and orientation become separate variables. Besides providing physical insight into the complex issue of charge collection, a goal of this work is to construct a set of numerical tools that can, by employing the input of a limited amount of experimental data, produce a continuous function that models the cross section, and can be used in the upset rate calculations. The approach leaves ion LET and orientation as separate variables. Furthermore, the curve is derived from physics and the model parameters correspond to physical observables. The predicted dependence of the cross section on LET is shown to agree with experimental data.

II. Description and Limitations of the Charge-Collection Model

A diffusion-only analysis might seem inappropriate in view of the fact that drift also contributes to charge collection. However, previous investigations have found that diffusion calculations can implicitly include drift subject to certain qualifications. What follows is a brief discussion on the relevent topics of the charge-collection model and qualifications used to derive the above assertion. For further details see [10], [14], and [15]. A limitation of the model is the presence of forward-biased structures is not considered, so the analysis does not apply to devices (e.g., SOI devices) that exhibit a strong bipolar gain amplification of collected charge. It is assumed that each sink for minority carriers is either an electrode contact or a reversed-biased p-n junction depletion region (DR) boundary (DRB). Charge collection is calculated for any selected DRB, and the calculations account for the fact that carrier removal by other sinks limits the charge available for collection by the selected DRB.

First consider the case in which the selected DR took a direct hit from a heavy ion. A rearrangement of liberated carriers, in response to the electric field in the DR, neutralizes the space charge formally in the DR, causing a DR collapse. For a typical low- to moderate-voltage microelectronic device, the number of carriers needed to do this is small enough that the intact part of the track, which is now completely outside the post-hit (collapsed) DR, is nearly all of the initial track. There is a displacement current during the collapse stage (the duration is measured in picoseconds), but this makes a negligible contribution to collected charge compared to the amount collected later. Nearly all charge collection occurs while the DR is recovering. The recovery stage begins with nearly all of the initial track outside of a very narrow DR. As recovery progresses, the DR expands (to regain its initial width) while carriers simultaneously move into the DR via drift/diffusion. The recovery is gradual enough that the displacement current is small compared to the flow (drift/diffusion) current, so there is a continuous flow current from one device terminal to another. However, whether a current is drift or diffusion depends on the location at which the current is evaluated, i.e., a current can be entirely drift at one location and a mixture of drift and diffusion at another location. The approximations used here can be explained by selecting the DRB as the location at which the current is calculated.

The first approximation ignores the DR expansion, so the DR is treated as a static system. Under static conditions, a reverse-biased DR blocks the majority carrier current because the strong electric field inside the DR prevents such carriers from traveling through. This means that the potential distribution in the quasi-neutral region outside the DR (which will be called the substrate for brevity) becomes whatever is required to produce the drift currents needed to make majority-carrier drift balance majority-carrier diffusion in the substrate near the DRB. Most charge collection occurs under high-density conditions (the carrier density greatly exceeds the doping density) both on the track and on the DRB. Such conditions, together with quasi-neutrality outside the DR, imply that the electron and hole densities have nearly equal values and gradients on the substrate side of the DRB, so electron and hole drift currents are in the ratio of the mobilities, and electron and hole diffusion currents are in the ratio of the mobilities. Therefore, majority-carrier drift being equal to majority-carrier diffusion implies that minority-carrier drift equals minority-carrier diffusion. However, the two minority-carrier currents add to instead of subtract from each other, so half of the total current at the DRB is minority-carrier drift and the other half is minority-carrier diffusion. Stated another way, the total current at the DRB is twice the minority-carrier diffusion current. If this current can be calculated, then the potential distribution in the substrate becomes incidental because it is enough to know that the potential distribution becomes whatever is needed to make the current equal to twice the minority-carrier diffusion current. The diffusion current is controlled by the gradient of the carrier density and this calculation requires additional approximations. The ambipolar diffusion equation is a good approximation for the purpose of calculating the carrier density, but boundary conditions are also needed. Although high-density conditions apply at the DRB, the carrier density there is still much smaller than it is elsewhere along the track. An approximation (which is not always good) is to treat the DRB as a sink for the purpose of estimating the carrier density gradient from the diffusion equation.

The above discussion started with a direct hit to the DR, but with or without a direct hit, the static approximation together with high-density conditions leads to the same conclusion; that the total current is twice the minority-carrier diffusion current.

The validity of this model was tested against a computer simulation that solved the drift/diffusion equations for a large-volume diode containing an ion track [10]. It is taken for granted here that the term “actual” is acceptable when referring to the simulation predictions, so we will use that term when referring to simulation predictions and say “calculated” when referring to predictions from the above model. In this comparison, the DR took a direct hit from the ion. The calculated collected charge up to a time t agreed well with the actual collected charge, providing that t is several nanoseconds or more. The agreement was very poor for earlier times (less than 1 ns). The actual current was much smaller than the calculated current at such times. The mathematical explanation is that, contrary to an assumption used for the model, the DRB is not sink-like at early times. The physical explanation is that the initial DR collapse is so great that the DR lost most of its built-in potential barrier, i.e., it became strongly forward biased. This produces

an emitter current (a forward current) that competes with the reverse current produced by the track below the DR. The model does not include a competing current, so it over-estimates the collected charge at early times. Fortunately, the contribution from early times to collected charge over much longer times is small enough for the model to be a good approximation for collected charge accumulated over several nanoseconds or more.

One limitation is that the model can only be used for devices having a long (several nanoseconds or more) charge-collection time (e.g., DRAMs). Another limitation could be removed, but is imposed here for computational convenience. The active layer must be thick enough so that it unnecessary to include any lower boundaries. Stated another way, the active layer must be thick enough so that the collection, by a selected sink, of charge liberated near the bottom is negligible, either because the collection is shared by many sinks and/or because of recombination (i.e., a finite diffusion length). Bulk DRAMs might be the only devices that can be treated, but the analysis is still useful because such devices are frequently used in space.

Note that a factor of two applied to the diffusion current (to include drift) is accompanied by another factor if the diffusion current is calculated by multiplying the carrier density gradient by the ambipolar diffusion coefficient instead of the minority-carrier diffusion coefficient. (It is mathematically convenient to use the same coefficient that appears in the diffusion equation.) The additional factor is the ratio of diffusion coefficients. However, these factors can be absorbed by the critical charge, so the equations in Section IV do not include them.

III. Definition of Directional Cross Section

By changing the order of integration (angles first and then LET, or vice-versa) and/or using a change in variables (e.g., to define an effective flux), there are a variety of equivalent ways to write an integral that combines device data with environmental data to obtain an upset rate, r. Depending on physical assumptions (e.g., the RPP model versus other), one way might be more convenient than another. The integral that is most convenient for the present work is from first principles:

$$r = \int_0^\infty \int_{-1}^{1} \int_0^{2\pi} \Phi\left(L,\theta,\phi\right) \sigma\left(L,\theta,\phi\right) d\phi \, d\left(\cos\theta\right) \, dL \tag{1}$$

where $\Phi\left(L,\theta,\phi\right)$ is the differential (in LET) directional flux, $\sigma\left(L,\theta,\phi\right)$ is the directional cross section, θ and ϕ are spherical coordinate angles, and L is particle LET. The directional cross section is experimentally defined as a number of counts divided by beam fluence where fluence is measured in a plane perpendicular to the beam, as opposed to the device plane. This is not the same as the cross section that is plotted in the traditional cosine-law format, in which fluence is measured in the device plane. The latter cross section is obtained by dividing the directional cross section by $\cos\theta$. Similarly, L is particle LET and is not the same as the "effective" LET that is plotted in the traditional cosine-law format. The effective LET is obtained by dividing the particle LET by $\cos\theta$. Plotting formats were compared in [13] for a particular DRAM (there is a mismatch between figures and captions in [13], and the caption that should be with Fig. 3 in [13] is actually with Fig. 6). The cosine-law format produced a badly scattered plot, while a plot of directional cross section versus particle LET showed much less scatter. The cosine-law format is clearly not a useful way to display these data, so in this paper, cross section refers to directional cross section and LET refers to particle LET.

If it were possible to experimentally measure the directional cross section for all directions and LETs, no device physics model would be needed because the above integral could be numerically evaluated using measured data. However, test ions at affordable (moderate-energy) facilities have limited ranges and this limits the tilt angles that produce meaningful data. Physical models are needed to extrapolate data from the limited angles that can be tested to the larger angles that are relevant in space. The objective of this paper is to suggest a possible method for predicting the directional cross section, at all angles and LETs, from either a knowledge of device physical parameters (if available) or from small-angle test data (via selecting physical parameters to fit data).

IV. The Diffusion Problem

It has been shown in [8] that all information regarding the ability of a DRAM cell to collect charge, via diffusion over a long enough period of time, is contained within the cell's charge collection efficiency function, $\Omega_\tau\left(\vec{x}\right)$. This function is a scalar potential that depends only on the device boundaries, and lifetime of the injected carriers, τ. Once determined for a particular geometry and τ, $\Omega_\tau\left(\vec{x}\right)$ can be used to calculate q_o for an arbitrary charge density, $\xi\left(\vec{x},t\right)$,

$$q_o = \int \Omega_\tau\left(\vec{x}\right) \xi\left(\vec{x},t=0\right) d^3x. \tag{2}$$

As shown in [8], $\Omega_\tau\left(\vec{x}\right)$ is defined to satisfy

$$\mathcal{L}\Omega_\tau\left(\vec{x}\right) = 0, \tag{3}$$

where $\mathcal{L}$ is the modified Helmholtz operator, $\left(\nabla^2 - \kappa^2\right)$, $\kappa^2 = \tau^{-1}D^{-1}$, and D is the diffusion coefficient.

The device under consideration is modeled as a silicon volume, occupying the half space $z \leq 0$, with the $z = 0$ plane coinciding with the upper boundary of the device where the ion strike enters the sensitive volume. This plane contains an infinite rectangular array of sinks, each representing the area of charge collection for a particular cell. The sinks are labeled $S_0, S_1, ...$, with the center of the sink of interest, S_0, being placed at the origin (see Fig. 1). The sinks have dimensions of $\{2a, 2b\}$ in the $\{x, y\}$ directions and are separated by the corresponding distances $\{\alpha, \beta\}$. The lack of a lower boundary on the device is justified if $\Omega_\tau \to 0$ for some $z \ll Z$, where Z is the substrate thickness. For the devices under study, this is a realistic simplification, however a future paper will introduce a lower device boundary and remove this limitation. As seen in (4), the boundary conditions on the sinks are of the Dirichlet type, while the areas between sinks are of the Neumann type.

$$\Omega_\tau\left(\vec{x} \in S_0\right) \quad = \quad 1$$

$$\begin{aligned} \Omega_\tau\left(\vec{x} \in S_i \notin S_0\right) &= 0 \\ \frac{\partial \Omega_\tau}{\partial \hat{n}}\left(\vec{x} \notin S_i\right) &= 0. \end{aligned} \tag{4}$$

The presence of the mixed boundary conditions complicates the solution of (3). However, if the orientation of the ion's momentum is restricted to be orthogonal to the upper plane of the device, realistic approximations can be used to derive an analytic function that relates LET and the upset cross sections, which is the subject of the following section.

V. Modeling Cross Sections Induced by Normal-Incident Ions

This section presents an analytic relationship between cross section and LET for a specific ion orientation: normal-incident ($\theta = \phi = 0$). This function utilizes three fitting parameters, which have physical interpretations, and can be optimized to predict cross sections for all LETs using just a handful of measurements.

The simple fitting function is given in (5), while the details of the derivation and assumptions used in solving (3) and (2) are shown in Appendix A.

$$L_N = A\sqrt{\sigma_N + B}e^{C\sqrt{\sigma_N + B}}, \tag{5}$$

where L_N and σ_N are the normal-incident LET and upset cross sections, respectively, while A, (MeV $\cdot$ cm/mg), B (cm^2), and C (cm^{-1}) are the fitting parameters. The parameter values pertaining to a particular device are determined via a χ^2 minimization.

To evaluate the usefulness of (5), a fit to the normal-incident Oki MSM514400 4 Mb DRAM data, first reported in [13], is performed. The resulting curve, along with the measured data are shown in Fig. 2. The resulting parameter values are: $A = 8.97$ MeV $\cdot$ cm/mg, $B = 0.00$ cm^2, and $C = 0.60$ cm^{-1}.

As seen in the figure, the curve successfully reproduces the data measured at normal-incidence. A Weibull curve (not shown) also fits the data very well. However, unlike the Weibull curve, the fitting parameters for the curve shown are related to physical device parameters (these relations are discussed in Appendix A.1). It should be possible to predict how the parameters will change when device characteristics are changed, but this assertion has not yet been tested so this is a subject for future work. This discussion focused on normal-incident data but a rate calculation requires a solution that applies to all angles, which is the subject of the next section.

VI. Modeling the Angular Dependence of Cross Sections

Again, the presence of the mixed boundary conditions complicates the solution to (3). Instead instead we choose to approximate $\Omega_\tau\left(\vec{x}\right)$, with a series solution, $\Psi_\tau\left(\vec{x}\right)$,

$$\Psi_\tau\left(\vec{x}\right) = \sum_i \sigma_i \psi_i\left(\vec{x}\right), \tag{6}$$

where the summation is over all sinks, and $\psi_i\left(\vec{x}\right)$ is the propagator integral for the modified Helmholtz equation,

$$\psi_i\left(\vec{x}\right) = \frac{1}{4\pi}\oint_{S_i'} dx'dy' \frac{\exp\left[-\kappa\sqrt{\left(x-x'\right)^2 + \left(y-y'\right)^2 + z^2}\right]}{\sqrt{\left(x-x'\right)^2 + \left(y-y'\right)^2 + z^2}}. \tag{7}$$

Note that $\Psi_\tau\left(\vec{x}\right)$ exactly solves (3) and is constrained by the Neumann conditions. However, the choice of the expansion coefficients, σ_i, which have the physical interpretation of the 'charge' densities that set up the collection efficiency 'field', determines how well the Dirichlet conditions are satisfied, and thus how accurate the approximation is.

In Fig. 1, a 5×5 grid is shown; however, for computations, a 7×7 array is used. The grid size can be extended to an arbitrary size, however 49 terms is adequate to ensure series convergence. The optimal expansion set, $\{\sigma_i\}$, is found via the calculus of variations, with the mathematical analysis given in Appendix B.

The values of $\{\sigma_i\}$ are dependent upon the geometry parameters (A, B, α, and β) as well as diffusion/recombination parameter, κ. For this study, we use $a = b = \alpha = \beta = 1$ and $\kappa = 0.1$. These dimensionless numbers refer to arbitrary units of the well array. For a device having 4 Mb distributed over an area of about 1 cm^2, the average distance between the centers of adjacent sinks should be about 5 μm, so the distance unit that should make the array conform to the actual device is roughly 2 μm. Therefore, $\kappa = 0.1$ corresponds to a diffusion length (equal to k^{-1}) of roughly 20 μm, which is believed to be credible in view of the fact that the parameter selection was somewhat ad hoc for this example.

The total charge collected via diffusion from an ion of LET$= L$ that strikes the device on the upper plane with coordinates, x, y, at an orientation of θ, ϕ is

$$\begin{aligned} q_o\left(x, y, \theta, \phi, L\right) = L\sum_i \sigma_i \int_0^\infty \psi(x + \lambda \sin\theta\cos\phi, \\ y + \lambda\sin\theta\sin\phi, -\lambda\cos\theta)d\lambda. \end{aligned} \tag{8}$$

For a particular choice of (θ, ϕ, L), the upset cross section is represented as the area, multipled by $\cos\theta$, bounded by the contour value $q_o = q_c$, where q_c is the critical charge needed for an upset. Contours for three ion orientations: $\theta = 0^o, 45^o, 60^o$ are shown in Figs. 3, 4, and 5. Each contour in the figures represents the cross section for a particular LET value. The corresponding LETs are: 1, 5, 10, 15, 20, ..., 60 MeV cm^2/mg, with the innermost contour being the LET = 1 MeV cm^2/mg cross section. Note that due to the choice of geometry parameters $a = b = \alpha = \beta$, these calculations are azimuthally symmetric, which is consistent with the Oki DRAM behavior.

VII. Comparison with Experimental Measurements

A consequence of numerically solving for the cross section is the ability to leave LET and orientation as independent variables, as opposed to combining them into an "effective LET".

As reported in [13], the OKi data is not 'well behaved' if interpreted via the cosine law. The un-transformed Oki data, along with the model's predictions are shown in Figs. 6, 7, and 8. Note the calculated curves for 0^o and 45^o reproduce the measurements. This is not merely an artifact of multiple adjustable parameters, because the family of curves that can be fit by our model is fairly restricted, so the agreement is encouraging. The prediction at 60^o is more troubling, but it is presently not clear whether the problem is with the prediction or with the data. It is well known that test data from moderate-energy facilities are meaningful only for restricted tilt angles because of ion range limitations. A bulk DRAM is expected to be the extreme case in terms of range requirements, i.e., the ion LET must be nearly constant over a very long path length in order for the range to be effectively infinite. Also, test data were obtained from BNL, which is one of the lower-energy facilities. The common practice is to vary the tilt angle up to 60^o, but it is unlikely that data abruptly change from good to bad at this angle. There might be a systematic trend from test limitations that is mild at 45^o but stronger at 60^o. This issue will be resolved in a future paper that will compare the present data with new data that will be obtained from a higher-energy facility. In the meantime, the good agreement with the normal-incident data encourages us to believe that the present work can serve as a foundation that future work can build upon.

VIII. Conclusions

Charge collection via diffusion incorporating carrier recombination is used to derive a 3 parameter analytic relationship between cross section and LET for normal-incident ions. This function is shown to accurately reproduce measurements for a real world device.

A generalized numerical solution to the diffusion equation incorporating mixed boundary conditions and carrier recombination is presented which is valid for all ion orientations. Using experimental data as input, it allows for the generation of a continuous cross section surface that is a function of both LET and orientation and can be used in upset rate calculations.

This technique has several advantages over the standard methodology of collecting data at several LETs and orientations, and combining the two independent variables into a single "effective LET" (via the cosine law). The cosine law is based on geometrical considerations with limited applicability to physical phenomena. In contrast, this work treats LET and orientation as separate environmental variables allowing for a more accurate prediction of the cross section across regimes of limited measurements, all of which results in more realistic error rates using less experimental measurements.

Appendix

A. Derivation of Normal-Incident Fitting Function

For a normal-incident ion, (2) simplifies to

$$q_o = aL \int \Omega_\tau (x, y, z)\, \mathrm{dz}, \tag{9}$$

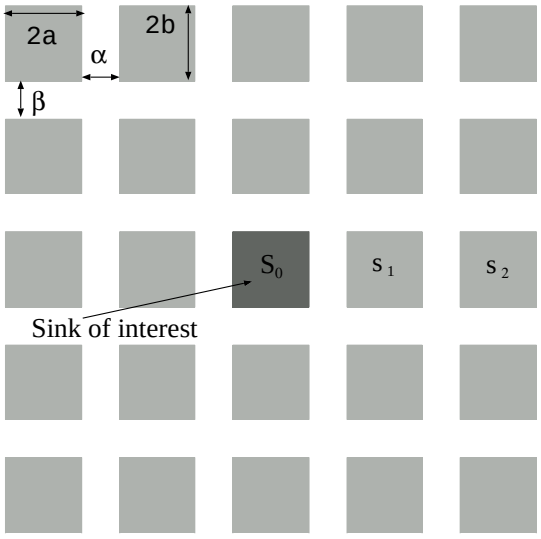

Fig. 1. The upper surface $(z = 0)$ of a memory device, covered by an infinite rectangular array of carrier sinks, labeled S_0, S_1, S_2, etc. Note the sink of interest, S_0, is located at the origin. The sinks have dimensions of a and b along the x and y axis, with spacings of α and β. The x axis lies along the horizontal, and the y along the vertical.

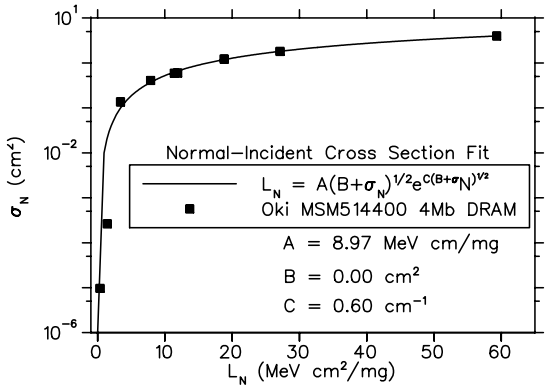

Fig. 2. Plot of the normal-incident fitting function (5) derived from (3) and the Oki MSM514400 4 Mb DRAM normal incident data. L_N and σ_N are the normal-incident LET and upset cross sections respectively. The values of the fitting parameters are also given. Note that no errors bars were reported for the Oki data.

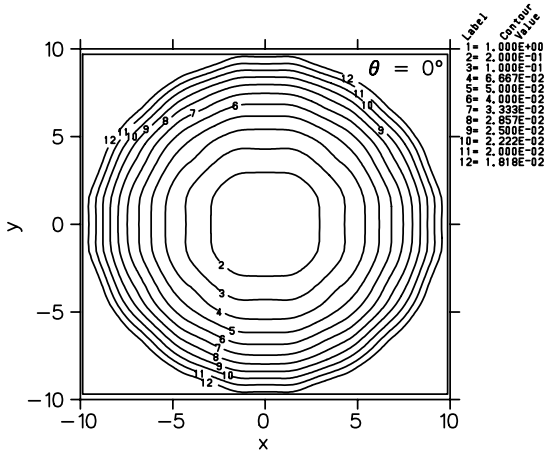

Fig. 3. Contours of charge collection for $\theta = 0^o$. The area bound by the contours are the cross sections at the various LETS listed in the text. The inverse of the values listed in the legend are the corresponding LETs of the contours. Note for $\theta = 0^o$ the cross sections are circular.

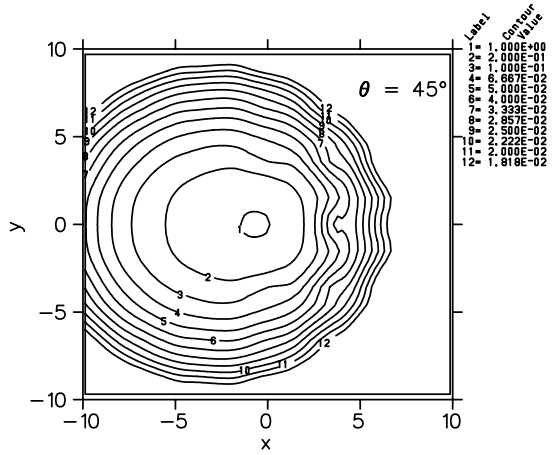

Fig. 4. Contours of charge collection for $\theta = 45^o$. The area bound by the contours are the cross sections at the various LETS listed in the text. The inverse of the values listed in the legend are the corresponding LETs of the contours.

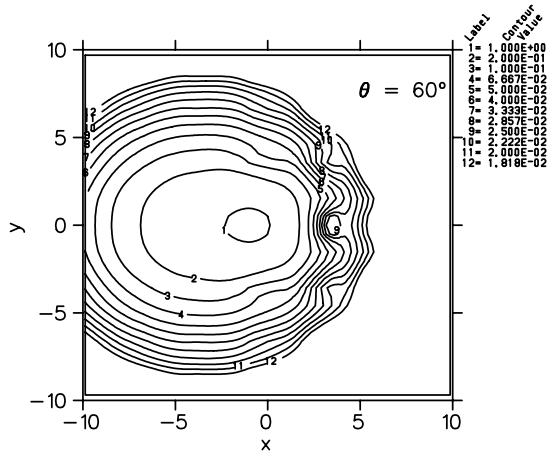

Fig. 5. Contours of charge collection for $\theta = 60^o$. The area bound by the contours are the cross sections at the various LETS listed in the text. The inverse of the values listed in the legend are the corresponding LETs of the contours.

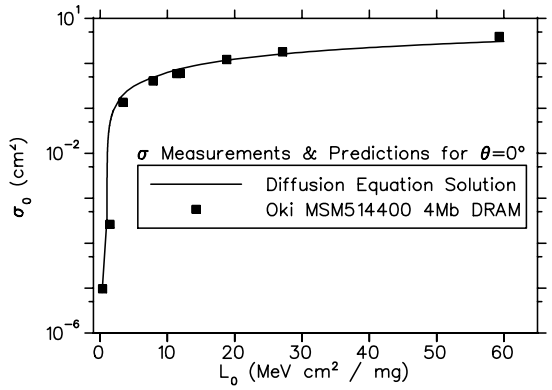

Fig. 6. Comparison of the upset cross sections predicted by diffusion as a function of LET and measurements of the Oki MSM514400 4 Mb DRAM, for $\theta = 0^o$. Note the theory successfully reproduces the data, implying that diffusion plays a critical role in in charge collection for this device.

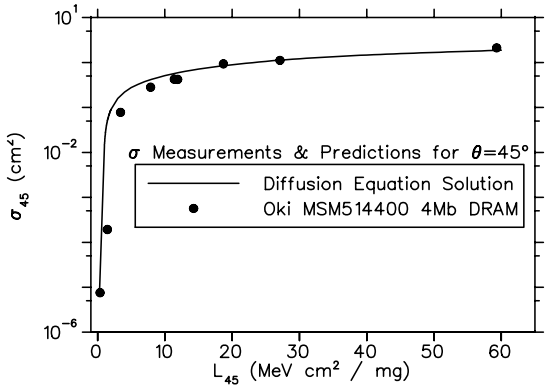

Fig. 7. Comparison of the upset cross sections predicted by diffusion as a function of LET and measurements of the Oki MSM514400 4 Mb DRAM, for $\theta = 45^o$. Note the theory successfully reproduces the data, implying that diffusion plays a critical role in in charge collection for this device.

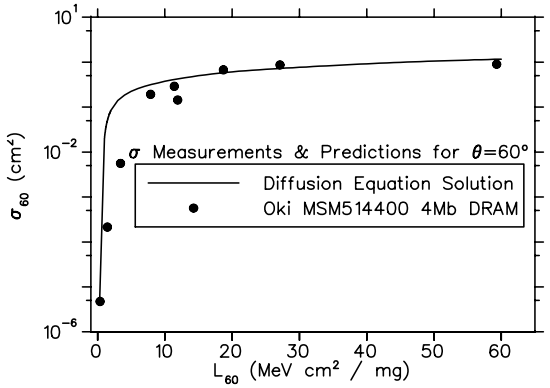

Fig. 8. Comparison of the upset cross sections predicted by diffusion as a function of LET and measurements of the Oki MSM514400 4 Mb DRAM, for $\theta = 60^o$. Note the scatter in the data would inhibit any 'smooth' function from precisely reproducing it.

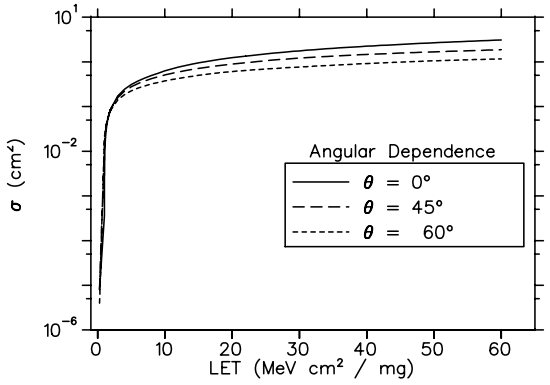

Fig. 9. The predicted cross sections for 3 angles of incidence $(\theta = 0^o, 45^o, 60^o)$. Note that keeping LET and angle of incidence as seperate variables is more successful at predicting cross sections than the standard method of combing them into "effective LET" via the cosine law.

where L is the LET and a is a unit conversion factor that converts LET, typically expressed in units of MeV cm^2/mg into μC/μm. Instead of solving a boundary value problem for Ω and then integrating, the algebra is more tractable if we solve for the integral of Ω directly. Define H by

$$H(x,y,z) \equiv \int_z^\infty \Omega(x,y,z')\,\mathrm{dz}'. \tag{10}$$

The objective is to solve for H. After doing that, q_o can be expressed in terms of H using (9) and (10) to arrive at

$$q_o = aLH(x,y,z). \tag{11}$$

To solve for H, integrate (3), while using $\frac{\partial\Omega}{\partial z} = 0$ as $z \to \infty$ to get

$$\nabla^2 H = \kappa^2 H, \tag{12}$$

i.e., H satisfies the same equation as Ω. Boundary conditions for H implied by (10) are

$$\frac{\partial H(x,y,z)}{\partial z}|_{z=0} = \Omega(x,y,0). \tag{13}$$

The solution of (12) and (13) is

$$\begin{aligned} H(x,y,z) &= \frac{1}{2\pi}\int \Omega(x',y',0)\,\mathrm{dx}'\mathrm{dy}' \\ &\quad \frac{\exp\left[-\kappa\sqrt{(x-x')^2+(y-y')^2+z^2}\right]}{\sqrt{(x-x')^2+(y-y')^2+z^2}}. \end{aligned} \tag{14}$$

Evaluating at $z = 0$ while using (11) gives

$$\begin{aligned} q_o(x,y) &= \frac{aL}{2\pi}\int \Omega(x',y',0)\,\mathrm{dx}'\mathrm{dy}' \\ &\quad \frac{\exp\left[-\kappa\sqrt{(x-x')^2+(y-y')^2+z^2}\right]}{\sqrt{(x-x')^2+(y-y')^2+z^2}}. \end{aligned} \tag{15}$$

Using the mean value theorem for integrals, we can write this as

$$\begin{aligned} q_o(x,y) &= \frac{\exp\left[-\kappa\sqrt{(x-x^*)^2+(y-y^*)^2+z^2}\right]}{\sqrt{(x-x^*)^2+(y-y^*)^2+z^2}} \\ &\quad \frac{aL}{2\pi}\int \Omega(x',y',0)\,\mathrm{dx}'\mathrm{dy}' \end{aligned} \tag{16}$$

for some suitable x^*, y^* which will depend on x, y. These coordinates are selected so that the coefficient to the integral in equation 16 is the average value of the coefficient to Ω in (15). One can think of x^* and y^* as average values of the source coordinates x' and y', with the average weighted by Ω, i.e., the average favors those values of x', y' at which $\Omega(x',y')$ is largest. Note that $\Omega(x',y')$ differs significantly from zero only when x', y' is on or near the sink of interest, so x^* and y^* are on the order of the sink dimensions (the origin of the coordinate system is centered on the sink of interest). Also note that

$$(x-x^*)^2 + (y-y^*)^2 \approx x^2 + y^2 + (x^*)^2 + (y^*)^2. \tag{17}$$

Another approximation is obtained by noting that x^* and y^* are important in (16) only when x and y are less than or on the order of the sink dimensions. Therefore an approximation for x^* and y^* that is good for small x and y can also be used for arbitrary x and y. One therefore approximates x^* and y^* with values that apply when $(x,y) = (0,0)$. In other words, a constant, B, can be defined as $(x^*)^2 + (y^*)^2$ is a constant, defined as

$$B \equiv \pi\left[(x^*)^2 + (y^*)^2\right]. \tag{18}$$

B is treated as a fitting parameter and (17) becomes

$$(x-x^*)^2 + (y-y^*)^2 \approx x^2 + y^2 + \frac{B}{\pi}. \tag{19}$$

Substituting in (16) gives

$$\begin{aligned} q_o(x,y) &= \frac{\exp\left[-\frac{\kappa}{\pi}\sqrt{\pi(x^2+y^2)+B}\right]}{\sqrt{\pi}\sqrt{pi(x^2+y^2)+B}} \\ &\quad \frac{aL}{2\pi}\int \Omega(x',y',0)\,\mathrm{dx}'\mathrm{dy}' \end{aligned} \tag{20}$$

For a given hit location, (x,y), we select L so that $q_o(x,y) = q_c$, the critical charge. Then $\pi(x^2+y^2)$ is the cross section, σ and (20) becomes

$$L = A\sqrt{\sigma+B}e^{C\sqrt{\sigma+B}}, \tag{21}$$

where A and C are additional constants defined by

$$A = \frac{2\sqrt{\pi}q_o}{a\int\Omega(x',y',0)\,\mathrm{dx}'\mathrm{dy}'} \tag{22}$$

and

$$C = \frac{\kappa}{\sqrt{\pi}}. \tag{23}$$

The equation used to fit data is 21 where A, B, and C are fitting parameters. The connection between the fitting parameters and physical parameters is given by (22) and (23) for A and C. The physical interpretation of B is a little more vague, but it is seen from (18) the B is on the order of the sink area.

The fitting parameters are related to physical parameters via the above equations only if the cross section is a per-bit cross section. Device cross sections can also be fit using (21), but the connection between fitting parameters and physical parameters is modified by the number of bits in the device.

B. Solution of charge

Consider two functions: Ω_τ and Ψ_τ, both of which are exact solutions of (3). Assume Ω_τ is exactly constrained by the mixed boundary conditions of (4). Construct Ψ_τ as in (6) and (7). Note Ψ_τ satisfies the Neumann boundary conditions, and we

will chose the optimum set of $\{\sigma_i\}$ to approximate the Dirichlet ones.

To quantify the approximation, define the following metric $\mathcal{M}$,

$$\mathcal{M} \equiv \int |\nabla\Omega - \nabla\Psi|^2 \, d^3x + \int \kappa^2 \, |\Omega - \Psi|^2 \, d^3x, \qquad (24)$$

where the integration is carried over the entire volume of the device. To find the expansion coefficients, we must minimize $\mathcal{M}$. Applying Greene's First Identity and it's corollary, we arrive at

$$\mathcal{M} = \oint_S \Omega \nabla\Omega . \hat{n} \mathrm{da} + \mathcal{J} \qquad (25)$$

where

$$\mathcal{J} \equiv 2 \oint_S \Omega \nabla\Psi . \hat{n} \mathrm{da} - \oint_S \Psi \nabla\Psi . \hat{n} \mathrm{da}. \qquad (26)$$

Note that the first term in (26) only contributes over the sink of interest S_0, thus

$$\mathcal{J} = 2 \oint_{S_0} \Omega \nabla\Psi . \hat{n} \mathrm{da} - \sum_i \oint_S \Psi \nabla\Psi . \hat{n} \mathrm{da}. \qquad (27)$$

To minimize $\mathcal{M}$, we will maximize $\mathcal{J}$. Note that since Ω is a field set up by the 'charges', $\{\sigma_i\}$ we can assume the E-field continuity conditions hold true, namely

$$\frac{\partial\Psi}{\partial z}|_{z=0} = -4\pi\sigma\,(x, y, 0)\,, \qquad (28)$$

thus $\nabla\Psi . \hat{n}$ contributes only over the wells. Let A_i be the area of the ith well, thus

$$\mathcal{J} = 2 \oint_{S_0} \sigma_0 \mathrm{da} + 4\pi \sum_i \oint_{S_i} \sigma_i \Psi\,(\vec{x})\,\mathrm{da}. \qquad (29)$$

Using (7) we have

$$\mathcal{J} = 2\sigma_0 A_0 - \sum_{i,j} \sigma_i \sigma_j R_{i,j}, \qquad (30)$$

where $R_{i,j}$ is a set of geometrical constants defined by

$$R_{i,j} = \oint_{S_i} \oint_{S_j} \frac{\exp\left[-\kappa\sqrt{(x-x')^2 + (y-y')^2}\right]}{\sqrt{(x-x')^2 + (y-y')^2}}. \qquad (31)$$

In order to maximize $\mathcal{J}$, set

$$\frac{\partial\mathcal{J}}{\partial\sigma_i} = 0 \qquad (32)$$

for all i. Substituting in (30) and performing some algebraic manipulations, we have

$$\sum_i \sigma_i R_{k,i} = A_0 \delta_{k,0}. \qquad (33)$$

Treating this as a system of linear equations, we solve for $\{\sigma_i\}$,

$$\vec{\sigma} = (R_{i,k})^{-1} A_0 \delta_{k,0} \qquad (34)$$

where $(R_{i,k})^{-1}$ is the inverse matrix of $R_{i,j}$. In practice, all integrations are carried out numerically.

REFERENCES

[1] E. L. Petersen, J. C. Pickel, E. C. Smith, P. J. Rudeck and J. R. Letaw, "Geometrical Factors in SEE Rate Calculations", IEEE Trans. Nucl. Sci., Vol. 40, No. 6, pp. 1888-1909, Dec 1993.

[2] L. W. Connell, P. J. McDaniel, A. K. Prinja, F. W. Sexton, "Modeling the Heavy Ion Upset Cross Section", IEEE Transactions on Nuclear Science, Vol. 42, No. 2, pp. 73-82, April 1995.

[3] L. W. Connell, F. W. Sexton, A. K. Prinja, "Further Development of the Heavy Ion Cross Section for Single Event Upset: Model (HICUP)", IEEE Transactions on Nuclear Science, Vol. 42, No. 6, pp 2026-2034, December 1995.

[4] P. E. Dodd, F. W. Sexton, P. S. Winkur, "Three-Dimensional Simulation of Charge Collection and Multiple-Bit Upset in Si Devices", IEEE Transactions on Nuclear Science, Vol. 41, No. 6, pp. 2005-2017, December 1994

[5] Y. Moreau, S. Duzellier, J. Gasiot "Evaluation of the Upset Risk in CMOS SRAM Through Full Three Dimensional Simulation", IEEE Transactions on Nuclear Science, Vol. 42, No. 6, pp. 1789-1796, December 1995

[6] J. Zoutendyk, L. Edmonds, and L. Smith, "Characterization of Multiple-Bit Errors and Single Ion Tracks in Integrated Circuits", IEEE Transactions on Nuclear Science, Vol. 36, No. 6, pp. 2267-2274, December 1989

[7] E. .C. Smith, E. .G. Stassinopoulos, K. LaBel, G. Brucker, C. M. Seidlick, "Application of a Diffusion Model to SEE Cross Sections of Modern Devices", IEEE Transactions on Nuclear Science, Vol. 42, No. 6, pp. 1772-1779, December 1995

[8] L. D. Edmonds "A Graphical Method for Estimating Charge Collected by Diffusion from and Ion Track", Vol. 43, No. 4, pp. 2346-2357, August 1996

[9] L. D. Edmonds "SEU Cross Sections Derived from a Diffusion Analysis", IEEE Transactions on Nuclear Science, Vol. 43, No. 6, pp. 3207-3217, December 1996

[10] L. D. Edmonds "A Time-Dependent Charge-Collection Efficiency for Diffusion", IEEE Transactions on Nuclear Science, Vol. 48, No. 5, pp. 1609-1622, October 2001

[11] S. Kirkpatrick, "Modeling Diffusion and Collection of Charge from Ionizing Radiation in Silicon Devices", IEEE Transactions on Electron Devices, Vol. 26, No. 11, pp. 1742-1753, November 1979

[12] S. Wouters, Diffusion-Based Silicon Radiation Detectors, Delft University Press, 1992

[13] S. M. Guertin, L. D. Edmonds, G. M. Swift, "Angular Dependence of DRAM Upset Susceptibility and Implications for Testing and Analysis" IEEE Transactions on Nuclear Science, Vol. 47, No. 6, pp. 2380-2385, December 2000

[14] L. D. Edmonds, "Charge Collection from Ion Tracks in Simple EPI Diodes," IEEE Transactions on Nuclear Science, Vol. 44, No. 3, pp. 1448-1463, June 1997.

[15] L. D. Edmonds, "Electric Currents Through Ion Tracks in Silicon Devices," IEEE Transactions on Nuclear Science, Vol. 45, No. 6, pp. 3153-3164, Dec. 1998.